Chemometrics and Intelligent Laboratory Systems 96 (2009) 227–238

Contents lists available at ScienceDirect

Chemometrics and Intelligent Laboratory Systems

journal homepage: www.elsevier.com/locate/chemolab

A simple correction method of inner filter effects affecting FEEM and its application to the PARAFAC decomposition

X. Luciani [a,b,*], S. Mounier [b], R. Redon [b], A. Bois [b]

[a] Laboratoire I3S, UMR6070, UNSA CNRS, 2000, route des Lucioles, BP 121, 06903 Sophia Antipolis Cedex, France
[b] Laboratoire PROTEE, USTV, BP 20132, 83957 La Garde Cedex, France

ARTICLE INFO

Article history:
Received 21 November 2008
Received in revised form 20 January 2009
Accepted 12 February 2009
Available online 25 February 2009

Keywords:
EEM
Inner filter effects
PARAFAC
3D fluorescence

ABSTRACT

In this paper we introduce a new inner filters correction method for standard fluorometer. The Controlled Dilution Approach (CDA) deals with highly absorbing solutions using the Fluorescent Excitation–Emission Matrix of a controlled weak dilution. Along with the nonlinear FEEM of the original solution, these information allow to estimate the linearized FEEM. The method relies on inner filter effects modelization. Beyond its numerical simplicity, the main interest is that CDA only requires fluorescence measurements. The method was validated using a set of known mixtures and a set of dissolved organic matter samples. In addition we show that the corrected FEEM can be used efficiently for advanced multilinear analysis. Therefore CDA is presented here as a relevant pretreatment to the PARAFAC decomposition of highly absorbing mixtures.

1. Introduction

1.1. Nonlinearities in fluorescence spectroscopy

Fluorescent molecular components (fluorophores) can be easily distinguished by their spectroscopic properties and more particularly by their fluorescence spectra [1]. Recent fluorometers provide successive measurements of the fluorescence intensity emitted by a solution of one or several fluorophores. By scanning excitation and emission wavelength domains, Fluorescent Excitation–Emission Matrices (FEEM) gather a lot of information about the solution. These spectra are now widely used in various scientific domains such as medicine [2], analytical chemistry [3] or environmental sciences [4,5].

Ideally, considering the FEEM (I_{3D}) of a single fluorophore, its norm is proportional to the fluorophore concentration in the solution and its pattern is given by the outer product between the excitation spectrum and the emission spectrum of the fluorophore. This is the classical linear model of fluorescence. However it is well known that its pertinence decreases with the concentration [6]. Actually, nonlinear deviations mean that the gradual absorption by the solution of both exciting and fluorescent lights cannot be neglected. These effects are known as inner filter effects and affect both I_{3D} norm and I_{3D} pattern. Therefore, in the presence of inner filter effects, one cannot deduce any correct information about the solution directly from I_{3D}.

Example of inner filter effects is given on Fig. 1. This example clearly shows that the FEEM pattern can be severely affected even in the simple case of a single fluorophore solution.

In other respects, considering several solutions of the same diluted fluorophore measured in different conditions, many other factors such as diffusion, temperature variations, pH variations, fluorescence quenching or ionic strength can affect the FEEM linearity [1]. In this work, we only focus on inner filter effects correction.

1.2. Inner filter effects correction

Inner filter effects are observed and studied for a long time now [7,8]. Two main correction methods are used to prevent these deviations. Since inner filter effects can be neglected for weak absorbances *i.e.* weak concentrations, a common procedure is to strongly dilute the solution until maximal absorbance is inferior than 0.1 [1]. There is an obvious drawback with this dilution method as a too strong diluting factor would severely reduce the signal to noise ratio. Moreover this procedure must be applied very carefully to avoid contamination or physico-chemical changes. Therefore, ensuring the linearity of the data set is no easy task. The second approach uses a mathematical model of inner filter effects [9–11]. Then one can deduce a correction factor in order to estimate element by element, a corrected FEEM (I_c) from I_{3D}. It is assumed that if the correction factor is suitable then I_c will follow the linear model. This approach relies on the Beer–Lambert law [1] which gives the elementary variation dI of the light intensity through an elementary optical path dl at wavelength λ:

$$dI = -I(\lambda)\alpha(\lambda)dl \quad (1)$$

* Corresponding author. Tel.: +33 492942792.
E-mail address: lucianix@gmail.com (X. Luciani).

0169-7439/$ – see front matter © 2009 Elsevier B.V. All rights reserved.
doi:10.1016/j.chemolab.2009.02.008

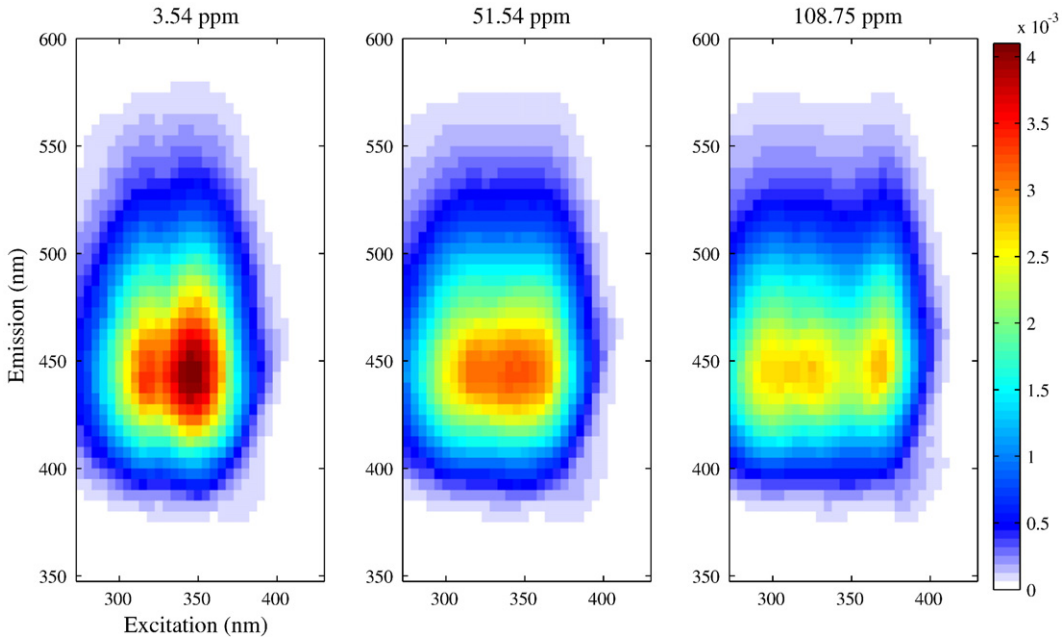

Fig. 1. Evolution of the quinine sulphate 3D spectrum for three different concentrations: 3.54 ppm (left spectrum), 51.54 ppm (middle spectrum), 108.75 ppm (right spectrum).

where α is the absorption coefficient of the solution. Then, the integrated law describes the light absorption through the entire optical path. If I_0 is the intensity of the exciting light, the transmitted intensity outside a cell of length l is simply given by the relation:

$$I(\lambda) = I_0(\lambda)e^{-\alpha(\lambda)l} = I_0(\lambda)10^{-A(\lambda)} \tag{2}$$

The absorbance spectrum of the solution is then defined by

$$A(\lambda) = \log_{10}\left(\frac{I_0(\lambda)}{I(\lambda)}\right) = \frac{l\alpha}{\log(10)} \tag{3}$$

Fig. 2 shows a schematic diagram of absorbance measurement. A is obtained by measuring the transmitted intensity through the diluted solution (I_T) and the transmitted intensity through the solvent (I_R) at successive wavelength:

$$A(\lambda) = \log_{10}\left(\frac{I_R(\lambda)}{I_T(\lambda)}\right) \tag{4}$$

In right angle fluorescence spectroscopy, classical model of inner filter effects is given by Eq. (5).

$$I_{3D}(\lambda_{ex}, \lambda_{em}) = I_c 10^{-\frac{A(\lambda_{ex}) + A(\lambda_{em})}{2}} \tag{5}$$

Thereby, one can use the measured absorbance spectrum to compute the correction factor and then deduce I_c. Similar methods were proposed in [12–14].

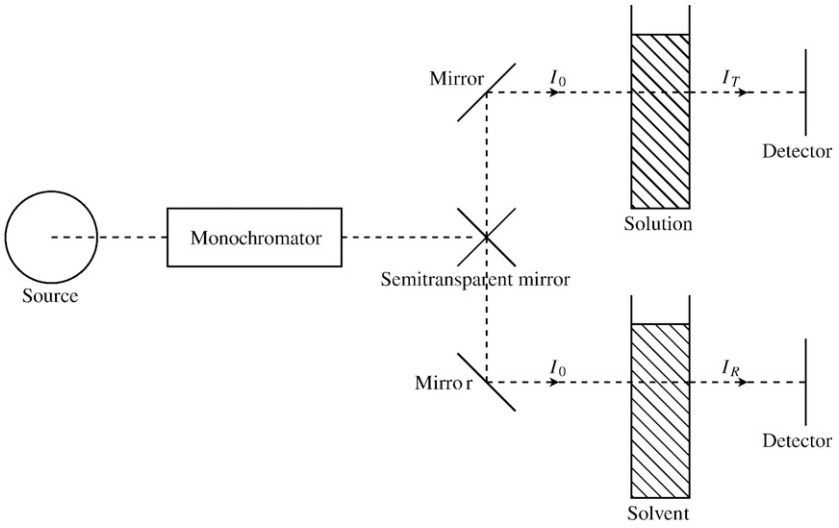

Fig. 2. Schematic diagram of absorbance measurement.

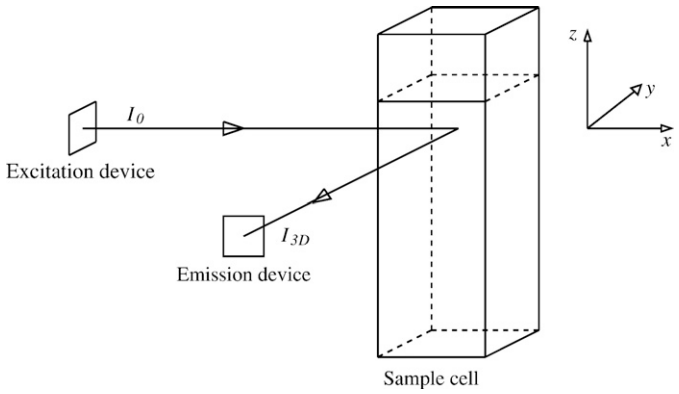

Fig. 3. Schematic diagram of right angle fluorescence measurement.

In the following, this approach will be identified as the Absorbance Correction Approach (ACA). ACA is commonly used in applicative papers dealing with fluorescence spectroscopy [15,16]. However absorbance measurement is much less sensitive than fluorescence measurement. In addition it requires another experimental device whose characteristics are different, introducing its own error in the chain. Finally, the short linear range of absorption measurement is another important drawback of ACA. In this work we propose an original correction method: the Controlled Dilution Approach (CDA) which combines the advantages of both methods. CDA uses the FEEM of a diluted solution instead of absorbance measurement in order to estimate I_c. The crucial point is that the dilution factor can be chosen small enough to avoid the drawback of the dilution approach. Indeed, the linearity of this second FEEM is not required. Consequently, CDA keeps the main advantage of ACA which is a very simple numerical correction, but it only requires fluorescence spectra. Analyzed solutions are generally mixtures of several fluorophores. Therefore, many applications involve a separation step to recover the underlying individual spectra and concentration profiles of each fluorophore. A number of chemometric methods were proposed in the literature in order to perform multilinear decompositions of FEEM [17–20]. Based on original works of Harshman [21], PARAllel FACtor analysis (PARAFAC) was introduced in this context by Bro [22]. During the last decade PARAFAC has proved to be the most relevant approach. For instance, in environmental sciences, it is currently the reference tool to characterize and trace Dissolved Organic Matter (DOM) [23–25]. In return, it does not take into account inner filter effects [26,27]. Consequently there is an irreversible loss of performance when dealing with highly absorbing mixtures.

Like other inner filter effects correction methods, CDA is independent of this separation step. However, we take into consideration that a large part of FEEM applications, uses this kind of decomposition. As a consequence, in order to ensure the reliability of CDA, we also present in this paper its performance as a PARAFAC pretreatment of highly absorbing mixtures.

1.3. Paper organization

CDA is detailed on Section 2 of this paper. First the modelization of inner filter effects is given in Section 2.1 then CDA is described on Section 2.2. Lastly, practical aspects of CDA are presented in Section 2.3 notably in the case of FEEM sets analysis. The PARAFAC application to the CDA corrected FEEM is shortly described.

In this work, CDA correction is experimentally tested on two very different sets of mixtures. The first set is composed of standard laboratory mixtures of fluorescein and quinine sulphate. Consequently, this first data set is used to strictly validate CDA and compare with classical ACA. On the other side, the second data set is constituted by unknown samples of DOM catchments and gives an example of how the method can help in a realistic case. Section 3 describes the experimental part of these tests. The results obtained on both data sets before and after the PARAFAC decomposition are presented and discussed in Section 4.

2. Theory

2.1. Modelization of inner filter effects

Like ACA, CDA relies on Eq. (5). Few authors give detailed mathematical justifications of this model, particularly in the most general case of 3D spectra of fluorophore mixtures. In this subsection a rigorous interpretation of Eq. (5) is proposed.

We consider here a mixture of N fluorophores. For each fluorophore n, we note c_n its concentration in the solution, $\varepsilon_n(\lambda_{ex})$ its molar extinction coefficient at the excitation wavelength λ_{ex}, Φ_n its quantum yield, $\gamma_n(\lambda_{em})$ its emission probability at wavelength λ_{em} and $\alpha_n(\lambda_{ex})$ its absorption coefficient which is equal to the product of c_n by $\varepsilon_n(\lambda_{ex})$. We assume that the absorption and emission spectra of fluorophore n are normalized values of respectively $\varepsilon_n(\lambda_{ex})$ and $\gamma_n(\lambda_{em})$. In the linear approximation, every fluorescing particle is treated equally as if the whole sample cell was an elementary point. In order to improve this model, one should take into account the particular geometry of the problem.

Fig. 3 recalls basically the experimental device of right angle standard fluorometers. The excitation light ($I_0(\lambda_{ex})$) is absorbed through the sample cell (length l) by the fluorophores, inducing the fluorescent light. Finally, a fraction ($I_{3D}(\lambda_{em})$) of the emitted signal is collected perpendicularly to the exciting beam. λ_{ex} and λ_{em} scannings allow to measure the FEEM.

In this study, several approximations were made. First of all, we took into consideration the symmetry of the problem, therefore the influence of the z spatial dimension was neglected.

Secondly, only two main optical paths were considered. They represent the excitation beam and emission beam in Fig. 4 scheme. This means that the fraction of the exciting light which does not reach the "influence zone" Z_e was neglected as well as the fluorescence light issued from the region outside Z_e. Then each elementary segment of the "excited face" of Z_e was supposed to receive the same energy from the rectilinear exciting beam. In the same way, we assumed that each elementary segment of the "emission face" of Z_e provides the same energy to the detector. Furthermore, diffusion and re-emission effects were also neglected. Actually we only consider the elementary optical paths represented in Fig. 5.

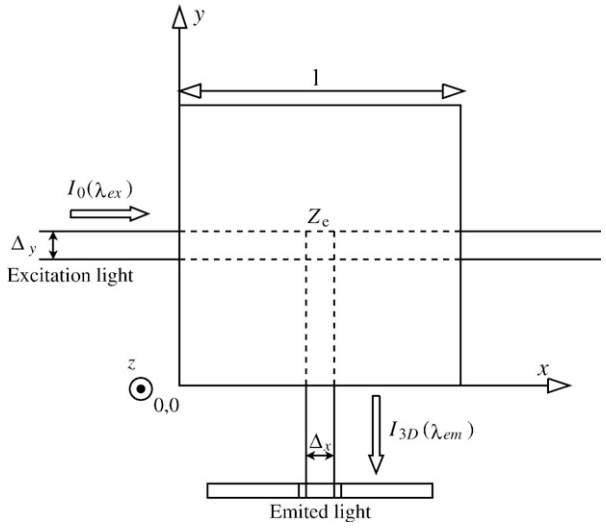

Fig. 4. Scheme of the sample cell, view from above.

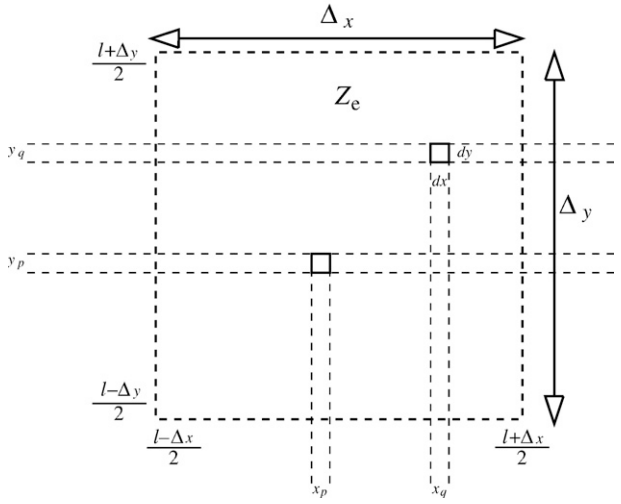

Fig. 5. Elementary cutting of the "influence zone" in the directions of exciting and emitted lights.

The integrated Beer–Lambert law describes the light absorption through the optical path. If I_0 is the light intensity at the point x_0 of the dilute solution, the intensity in x is simply given by the relation: $I = I_0 e^{-\alpha(\lambda_{ex})(x-x_0)}$ where α is the mixture total absorption coefficient: $\alpha = \Sigma_n \alpha_n$. The influence zone was divided into horizontal and vertical elementary strips of respective dimension $dy \times l$ and $l \times dx$. Then each horizontal strip receives an equal elementary fraction of the exciting light: $\frac{dy I_0}{\Delta_y}$ and the Beer–Lambert law quantifies the intensity transmitted to x. A fraction $\alpha_n dx$ is absorbed by fluorophore n, and the total intensity absorbed by fluorophore n in the "influence zone" (I_{An}) is given by:

$$I_{An}(\lambda_{ex}) = \frac{dy I_0}{\Delta_y} \alpha_n(\lambda_{ex}) \int_{\frac{l-\Delta_x}{2}}^{\frac{l+\Delta_x}{2}} e^{-\alpha(\lambda_{ex})x} dx \tag{6}$$

$$I_{An}(\lambda_{ex}) = 2\frac{I_0}{\Delta_y \alpha(\lambda_{ex})} \alpha_n(\lambda_{ex}) e^{-\frac{\alpha(\lambda_{ex})l}{2}} \sinh\left(\frac{\alpha(\lambda_{ex})\Delta_x}{2}\right) dy \tag{7}$$

The fluorescence signal emitted by the dy strip at wavelength λ_{em} is equal to $\Sigma_n \Phi_n \gamma_n(\lambda_{em}) I_{An}(\lambda_{ex})$ and the Beer–Lambert law integrated on all the elementary horizontal strips gives the ratio of the fluorescence signal transmitted outside the sample cell in the y direction, $I_{3D}(\lambda_{ex}, \lambda_{em})$.

$$I_{3D}(\lambda_{ex}, \lambda_{em}) = \int_{\frac{l-\Delta_y}{2}}^{\frac{l+\Delta_y}{2}} \sum_n \Phi_n \gamma_n(\lambda_{em}) I_{An}(\lambda_{ex}) e^{-\alpha(\lambda_{em})y} \tag{8}$$

$$I_{3D}(\lambda_{ex}, \lambda_{em}) = \frac{4 I_0 e^{-\frac{\alpha(\lambda_{ex})l}{2}} \sinh\left(\frac{\alpha(\lambda_{ex})\Delta_x}{2}\right) e^{-\frac{\alpha(\lambda_{em})l}{2}} \sinh\left(\frac{\alpha(\lambda_{em})\Delta_y}{2}\right)}{\Delta_y \alpha(\lambda_{ex}) \alpha(\lambda_{em})} \sum_n \alpha_n(\lambda_{ex}) \Phi_n \gamma_n(\lambda_{em}) \tag{9}$$

$\frac{\alpha(\lambda_{ex})\Delta_x}{2}$ and $\frac{\alpha(\lambda_{em})\Delta_y}{2}$ are supposed to be small enough to make the following approximation:

$$I_{3D}(\lambda_{ex}, \lambda_{em}) = I_0 \Delta_x \left(\sum_n \alpha_n(\lambda_{ex}) \Phi_n \gamma_n(\lambda_{em}) \right) e^{-\frac{\alpha(\lambda_{ex})l}{2}} e^{-\frac{\alpha(\lambda_{em})l}{2}} \tag{10}$$

Then we can define $g = 1/2$ and $G_n = I_0 \Delta_x \Phi_n$. This leads to the final expression of the model:

$$I_{3D}(\lambda_{ex}, \lambda_{em}) = \left(\sum_{n=1}^{N} G_n c_n \varepsilon_n(\lambda_{ex}) \gamma_n(\lambda_{em}) \right) \prod_{n=1}^{N} e^{-g(c_n \varepsilon_n(\lambda_{ex}) + c_n \varepsilon_n(\lambda_{em}))} \tag{11}$$

In the following we define

$$L(\lambda_{ex}, \lambda_{em}) = \sum_{n=1}^{N} G_n c_n \varepsilon_n(\lambda_{ex}) \gamma_n(\lambda_{em}) \tag{12}$$

then we have

$$I_{3D}(\lambda_{ex}, \lambda_{em}) = L e^{-g(c_n \varepsilon_n(\lambda_{ex}) + c_n \varepsilon_n(\lambda_{em}))} \tag{13}$$

This equation is clearly equivalent to Eq. (5) with $I_c = L$. Its first order approximation is justified for small enough concentrations. In this case, since the exponential term tends to 1 one obtains the linear model of fluorescence.

Correction of inner filter effects simplifies spectral analysis. It is interesting to note that their modelization is also used in another context. Actually, a recent article [28] highlighted the major contribution of inner filter effects in the phenomenon of concentration-dependent red-shift [29,30]. In this work, a similar model has been successfully used to optimize synchronous fluorescence spectroscopy of concentrated mixtures of fluorophores.

2.2. Controlled Dilution Approach

The previous model describes nonlinear effects but the related equation can still be considered as a bilinear decomposition involving some modified individual spectra $\varepsilon'_n(\lambda_{ex})$ and $\gamma'_n(\lambda_{em})$:

$$I_{3D}(\lambda_{ex}, \lambda_{em}) = \sum_{n=1}^{N} \varepsilon'_n(\lambda_{ex}) \gamma'_n(\lambda_{em}) \tag{14}$$

with,

$$\varepsilon'_n(\lambda_{ex}) = G_n c_n \varepsilon_n(\lambda_{ex}) e^{-\sum_{p=1}^{N} g c_p \varepsilon_p(\lambda_{ex})} \tag{15}$$

$$\gamma'_n(\lambda_{em}) = \gamma_n(\lambda_{em}) e^{-\sum_{p=1}^{N} g c_p \varepsilon_p(\lambda_{em})} \tag{16}$$

It is well known that bilinear decompositions have an infinite number of equivalent solutions in the least square sense. Therefore, without additional information, no mathematical tool can diagnose whether a FEEM is affected by inner filter effects or not. *A fortiori* additional information are also needed to correct inner filter effects. In ACA this information is the solution absorbance spectrum. This section shows how the correction can be made with fluorescent spectra only.

According to Eq. (11) the FEEM I_{3D} of an N fluorophores mixture is the product of a linear (L) term in respect of concentrations and spectra by a nonlinear one, denoted H:

$$H(\lambda_{ex}, \lambda_{em}) = \prod_{n=1}^{N} \exp(-g(c_n \varepsilon_n(\lambda_{ex}) + c_n \varepsilon_n(\lambda_{em})) \tag{17}$$

So we can write:

$$I_{3D}(\lambda_{ex}, \lambda_{em}) = L(\lambda_{ex}, \lambda_{em}) H(\lambda_{ex}, \lambda_{em}) \tag{18}$$

Now, let I_{3Dp} be the FEEM of the same mixture, diluted by a factor p, then we have:

$$I_{3Dp}(\lambda_{ex}, \lambda_{em}) = \left(\sum_{n=1}^{N} G_n \frac{c_n}{p} \varepsilon_n(\lambda_{ex}) \gamma_n(\lambda_{em}) \right) \prod_{n=1}^{N} e^{-g\left(\frac{c_n}{p} \varepsilon_n(\lambda_{ex}) + \frac{c_n}{p} \varepsilon_n(\lambda_{em})\right)} \tag{19}$$

$$I_{3D_p}(\lambda_{ex}, \lambda_{em}) = \frac{1}{p} L(\lambda_{ex}, \lambda_{em}) H^{\frac{1}{p}}(\lambda_{ex}, \lambda_{em}) \tag{20}$$

Table 1
Concentrations, maximal absorbances and mean absorbances of the original solutions of quinine sulphate and fluorescein.

Solution	S_1^1	S_1^2	S_1^3	S_1^4	S_1^5	S_1^6	S_1^7
c_{SQ} (ppm)	0	11.02	32.6	54.38	76.15	97.73	108.75
c_F (ppm)	83.15	74.72	58.23	41.58	24.92	8.43	0
Absorbance max.	2.30	2.18	1.83	1.32	1.17	1.38	1.47
Mean absorbance.	0.42	0.40	0.37	0.33	0.29	0.27	0.24

Concentrations in quinine sulphate (c_{SQ}) and fluorescein (c_F) are given in parts per million (ppm). Maximum and mean value of absorbance are relative to the 275 to 500 nm excitation range.

The analytical resolution of Eqs. (18) and (20) gives

$$L(\lambda_{ex},\lambda_{em}) = \left(\frac{\left(pI_{3D_p}(\lambda_{ex},\lambda_{em})\right)^p}{I_{3D}(\lambda_{ex},\lambda_{em})}\right)^{\frac{1}{p-1}} \quad (21)$$

$$H(\lambda_{ex},\lambda_{em}) = \left(\frac{I_{3D}(\lambda_{ex},\lambda_{em})}{pI_{3D_p}(\lambda_{ex},\lambda_{em})}\right)^{\frac{p}{p-1}} \quad (22)$$

The L term is the corrected FEEM estimated by CDA, corresponding to the linear model of fluorescence. As previously mentioned, the correction only requires the original FEEM and the diluted FEEM and the value of the dilution factor p.

The sensitivity of the estimator of L to p is difficult to quantify. A first order approximation of the variability of L (Δ_L) leads to:

$$\frac{\Delta_L}{L} = \frac{\left(p - 1 - \log(p) - \log\left(I_{3D_p}\right) + \log(I_{3D})\right)\Delta_p}{(p-1)^2}$$

According to this equation, a high factor should be preferred. However it would involve the drawbacks of a strong dilution (see Section 1.2). Finally, we advocate for a dilution factor corresponding to the simplest dilution process, thus the experimental uncertainty Δ_p is minimized. This was the case for all the experiments presented in this study.

Owing to the term by term division in Eq. (21), noisy values in the measured FEEM could affect the estimation of L. Actually if the division involves two small values relatively to the noise level, some very narrow and localized peaks can appear. Fluorescent spectroscopy is a very sensitive technique therefore this kind of deviation is rarely observed in practical situations. Otherwise those peaks appear outside the main fluorescing areas. In consequence, they can be easily detected and filtered without damaging the fluorescent peaks.

2.3. CDA and multilinear analysis of concentrated fluorescing mixtures

We consider now a set of I mixtures and $c_n(i)$ denotes the concentration of fluorophore n in mixture i. CDA methodology is simple, the correction is done sample by sample. The first step consists in choosing the dilution factor p for each sample (see the end of Section 2.2). Obviously the same value can be used for every sample. Then, the corresponding controlled dilution is performed and both FEEM I_{3D} and I_{3Dp} are measured. Before correction, Rayleigh and Raman scatters must be corrected carefully on each FEEM. This is the end of the experimental and pre-processing steps.

Finally, for each sample i, the estimation $L(i, \lambda_{ex}, \lambda_{em})$ of the linearized FEEM is obtained directly from Eq. (21). At this stage, the correction of the inner filter effects is completed.

Actually we have to take into account measurement and modelization errors. In addition we can define $\tilde{c}_n(i) = G_n c_n(i)$. Therefore in practice, definition (12) is rewritten:

$$L(i,\lambda_{ex},\lambda_{em}) = \sum_{n=1}^{N} \tilde{c}_n(i)\varepsilon_n(\lambda_{ex})\gamma_n(\lambda_{em}) + E(i,\lambda_{ex},\lambda_{em}) \quad (23)$$

where E is the error term. Eq. (23) is a rank N decomposition of the 3 way tensor L or in other words a 3-way PARAFAC model of rank N. For each fluorophore n, the loading vectors of the decomposition $\tilde{c}_n$, ε_n, and γ_n are linearly linked to its concentration profile, its excitation spectrum and its emission spectrum respectively. Moreover, the solution of this decomposition is unique up to trivial scaling and position indeterminacy [31,32]. Finally, several efficient algorithms were proposed and compared for the estimation of the loading vectors. These are largely described in the literature [33–35]. Those three physical, mathematical and practical reasons made the PARAFAC decomposition the most suitable tool for analysing linear(ized) FEEM. Tutorials and examples of PARAFAC application to FEEM analysis can be found elsewhere [36,22,37].

Eventually, the PARAFAC decomposition can be run normally on the corrected FEEM set in order to find out real individual spectra and concentration profiles of each fluorophore.

3. Experimental

3.1. Data set 1, standard mixtures

Seven solutions (S_1^i, $i=1\ldots,7$) with different concentrations of fluorescein (Aldrich) and quinine sulphate (Merkc) were prepared in 0.1 M H_2SO_4 (Aldrich) in order to validate the correction method. All chemicals are analytical grade. Concentrations in fluorescein and quinine sulphate are given in Table 1 along with solution absorbances. These two fluorophores and their concentrations in the solutions were chosen because of their good fluorescing ability and their overlapped spectra in order to emphasize inner filter effects.

Seven twice diluted solutions (S_{1D}^i, $i=1\ldots,7$) were obtained by mixing equal volumes of initial solutions S_1^i and 0.1 M of H_2SO_4. Table 2 gives the actual value of the dilution factor for the seven solutions and the standard deviation due to the pipet precision.

Reference solutions (S_{1R}^i, $i=1\ldots,7$) were obtained by diluting 100 µL of S_1^i in 3000 µL of 0.1 M of H_2SO_4. In this case of simple mixtures, this dilution prevents inner filter effects without physico-chemical changes.

All measured spectra were obtained with a fluorometer Hitachi F4500. FEEM of the three solutions sets S_1, S_{1D} and S_{1R}, were recorded at 30,000 nm/min scan speed from 350 to 700 nm in emission by step of 5 nm and for excitation wavelength from 275 to 500 nm by step of 5 nm. Excitation and emission bandwidth were 5 nm. Fluorescence intensity was corrected from PM response using manufacturer setting. Data for FEEM treatment were extracted by FLWinLab software for emission and excitation range stepped every 5 nm. Rayleigh and Raman scatters were removed numerically by the method proposed by Zepp in [38]. In the following, measured FEEM from original, diluted and reference solution i will be referred as I_{1U}^i, I_{1D}^i and I_{1R}^i respectively. Absorption spectra of solutions S_1 were obtained from transmittance spectra recorded with absorbance mode of the F4500 (speedscan 240 nm/min) from 200 to 800 nm with 5 nm bandwidths in excitation and emission. 2D reference spectra of fluorescein and quinine sulphate were recorded from S_{1R}^1 and S_{1R}^7 respectively, at 240 nm/min scan speed by step of 1 nm with 5 nm bandwidth in excitation and 2.5 nm bandwidth in emission. Quinine sulphate ($I_{SQ\text{-}ex}$) and fluorescein ($I_{F\text{-}ex}$) excitation spectra were recorded from 275 to 500 nm at 450 nm and 510 nm emission wavelength respectively. Their emission spectra

Table 2
Dilution factors used for the seven solutions of fluorescein and quinine sulphate.

Solution	S_{1D}^1	S_{1D}^2	S_{1D}^3	S_{1D}^4	S_{1D}^5	S_{1D}^6	S_{1D}^7
p	2.11	2.08	2.07	2.07	2.07	2.08	2.11
σ_p	0.034	0.032	0.030	0.029	0.030	0.032	0.034

σ_p is the estimated standard deviation of the dilution factor due to the experimental dilution.

($I_{SQ\text{-}em}$ and $I_{F\text{-}em}$) were recorded from 350 to 700 nm at 340 nm and 440 nm excitation wavelength respectively.

I_{1R} and I_{1U} compose the groups of reference and uncorrected FEEM respectively. Using absorption spectra in Eq. (5), we could compute the ACA corrected FEEM (I^i_{1ACA}) from I^i_{1U}, $i=1\ldots, 7$. In the same way, using I^i_{1D} in Eq. (21) with dilution factor values of Table 2, we could apply CDA to I^i_{1U} and compute the CDA corrected FEEM (I^i_{1CDA}), $i=1\ldots, 7$. I_{1ACA} and I_{1CDA} compose the groups of ACA and CDA corrected FEEM respectively.

These four groups of FEEM are considered as four 3-way tensors of dimensions $7\times46\times51$. Trilinear decompositions of these tensors were performed with the PARAFAC-ALS algorithm of the nway toolbox for Matlab [39].

3.2. Data set 2, unknown samples

The second data set is composed of FEEM obtained from eleven samples of concentrated humic acid solutions which were extracted from catchments of Cameron soils. For each sample, 1 g of soil was extracted by 30 mL of HCl (1 M) solution. After separation, the supernatant solution was cleaned on XAD-8 resin and stored at 4 °C in dark. The resting soil was then extracted with 30 mL of 1 M NaOH solution. After separation, this second supernatant contains humic acid substance. Purification was done by acidic precipitation and sodic redissolution. Humic acid gave dark brown solution and fulvic acid yellow solution. Original solutions (S^i_2, $i=1\ldots, 11$), were obtained by diluting 100 µL of the extracted solutions in 3000 µL of 0.1 M NaOH

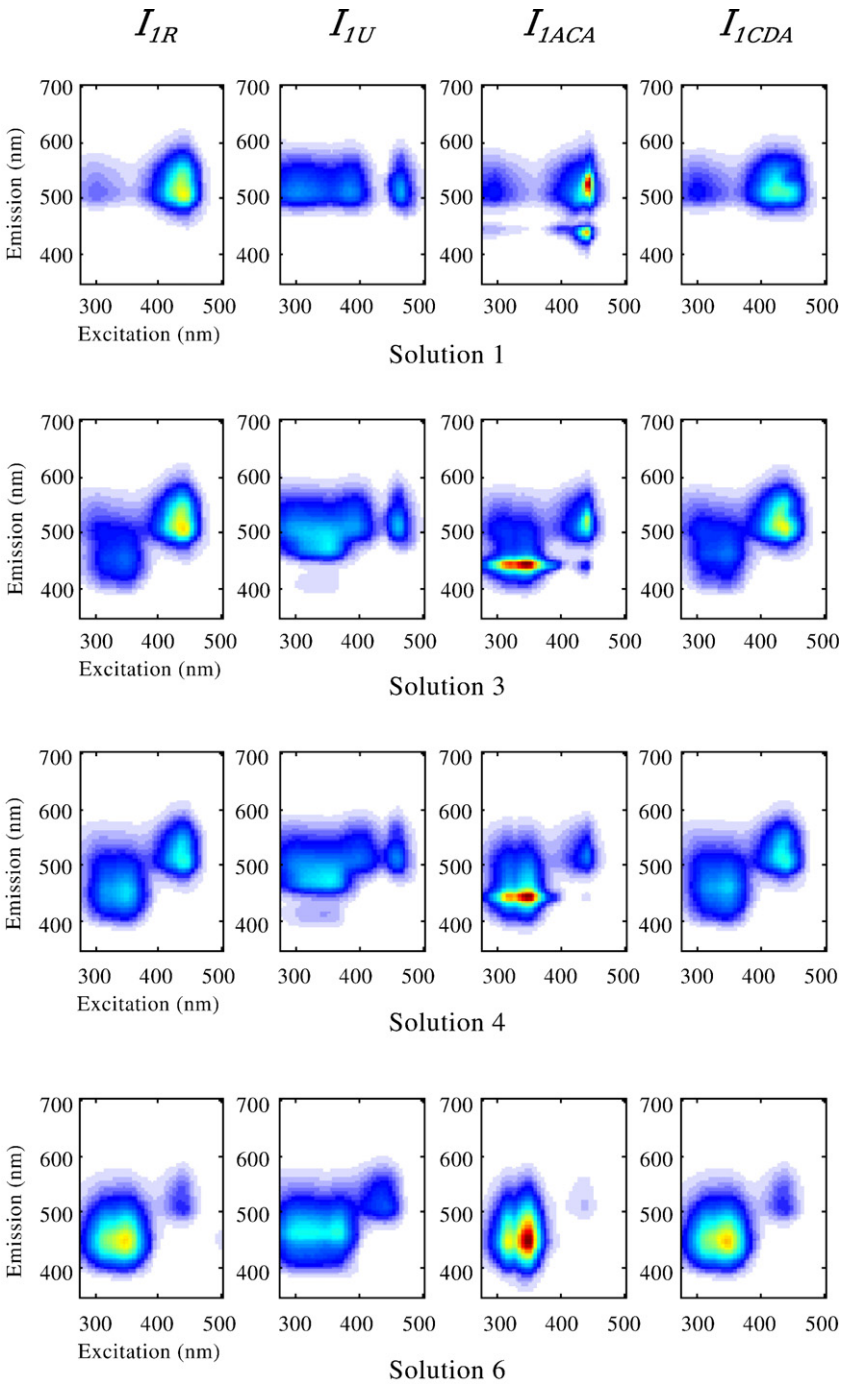

Fig. 6. Illustrations of I_{1R}, I_{1U}, I_{1ACA} and I_{1CDA} for solutions 1, 3, 4 and 6 of data set 1.

Table 3
Comparison of the relative squared residual error terms (in %) for the seven solution of data set 1.

Solution	1	2	3	4	5	6	7
r_{1U}	117	109	81	46	29	20	13
r_{1ACA}	31	38	59	33	14	7	8
r_{1CDA}	11	5	2	1.8	0.3	0.06	0.03

buffer. All chemicals are analytical grade. Eleven twice diluted solutions in 0.1 M NaOH buffer (S^i_{2D}, $i=1\ldots,11$) were also prepared. Finally, reference solutions without inner filter effect (S^i_{2R}, $i=1\ldots,11$) were obtained by 15 times dilutions of S^i_{2D}.

FEEM of S^i_2 (I^i_{2U}), S^i_{2D} (I^i_{2D}) and S^i_{2R} (I^i_{2R}) were recorded for $i=1\ldots,11$, at 30,000 nm/min scan speed from 340 to 650 nm in emission for excitation wavelength from 240 to 600 nm, by emission and excitation step of 5 nm and with 10 nm bandwidth in excitation and 5 nm bandwidth in emission. Rayleigh and Raman scatters were consistently corrected [38].

I_{2R} and I_{2U} compose the groups of reference and uncorrected FEEM respectively. Using I^i_{2D} in Eq. (21) with $p=2$, we could apply CDA to I^i_{2U} and compute the CDA corrected FEEM (I^i_{2CDA}), $i=1\ldots,11$. I_{2CDA} compose the group of CDA corrected FEEM. Comparison with ACA was not made on this data set. Hence, three tensors of dimensions $11\times73\times63$ were obtained and decomposed by PARAFAC-ALS [39].

4. Results and discussion

In the following the PARAFAC applications to uncorrected, reference, ACA corrected and CDA corrected groups of FEEM will be referred as U-PARAFAC, R-PARAFAC, ACA-PARAFAC and CDA-PARAFAC respectively.

4.1. Data set 1

Each CDA corrected FEEM (I^i_{1CDA}, $i=1\ldots7$) are firstly compared to I^i_{1R}, I^i_{1U} and I^i_{1ACA}. Representative examples of these FEEM are presented on Fig. 6 for $i=\{1,3,4,6\}$. In these examples, CDA provides satisfying estimations of the reference FEEM in spite of a small distortion in the fluorescein peak (440/510 nm), particularly on I^1_{1CDA}. In order to quantify these comparisons three relative squared residual error terms (r^i_{1CDA}, r^i_{1U} and r^i_{1ACA}) were computed as follow for each solution i and stored in Table 3.

$$r^i_{1CDA}=\frac{\sum_{j,k}\left(I^i_{1R}(j,k)-I^i_{1CDA}(j,k)\right)^2}{\sum_{i,j}I^i_{1R}(j,k)^2} \quad (24)$$

$$r^i_{1U}=\frac{\sum_{j,k}\left(I^i_{1R}(j,k)-I^i_{1U}(j,k)\right)^2}{\sum_{j,k}I^i_{1R}(j,k)^2} \quad (25)$$

$$r^i_{1ACA}=\frac{\sum_{j,k}\left(I^i_{1R}(j,k)-I^i_{1ACA}(j,k)\right)^2}{\sum_{j,k}I^i_{1R}(j,k)^2} \quad (26)$$

The significance of the nonlinear term in Eq. (11) increases with the solution absorbance. Therefore, comparing Tables 1 and 3, there is an obvious correlation between r_{1U} and the mean absorbances as both values decrease regularly from solutions 1 to 7. The same observation holds true regarding r_{1CDA}. The correlation is less apparent for r_{1ACA} but globally the error is greater for solutions 1 to 4 than for the least absorbing solutions. r_{1U} values are comprised between 13% and 117%. After CDA correction, these boundary values decreased to 0.03% and 11% respectively. These results are very satisfying for solutions 2 to 7. The first solution shows a stronger error but there is still a clear improvement in comparison of the original FEEM. CDA results are always clearly better than ACA ones. Actually, in the more favourable case in respect to ACA results (solution 1), r_{1ACA} is almost 3 times greater than r_{1CDA}.

These results showed that CDA provided a better estimation of I_{1R} than ACA. In order to verify if CDA correction is satisfying for further analysis, the PARAFAC-ALS algorithm was applied to the four groups of FEEM. For each group, the core consistency diagnostic (CORCONDIA) [40] suggested two as the right number of components. Consequently, each PARAFAC decomposition provides an estimation of the quinine sulphate and fluorescein excitation and emission spectra and an estimation of their relative concentrations trough the data set. After normalisation, the relative squared errors (r^c, r^{ex} and r^{em}) between the PARAFAC loadings and the real variables are compared on Tables 4–6. In the case of the spectral loadings, two other spectroscopic criteria are also used: the relative error to the maximum value of the spectrum and the shift on the position of the maximum. In addition, loadings obtained from U-PARAFAC and CDA-PARAFAC are shown on Figs. 7–9, along with real spectra and profiles. A first global remark should be made: the perfect agreement on the three modes between the real variables and R-PARAFAC loadings demonstrates that estimation errors of U-PARAFAC, ACA-PARAFAC and CDA-PARAFAC are mainly due to inner filter effects and not to the PARAFAC decomposition.

Results for the concentration mode are presented in Table 4 and Fig. 7. The shape of the concentration profile of the quinine sulphate is slightly affected by filter effects ($r^c_{1U}=8.3\%$). However CDA-PARAFAC gives much more accurate results for each solution ($r^c_{1CDA}=0.2\%$). ACA-PARAFAC is also satisfying but it is not as efficient as CDA. The concentration profile of the fluorescein is more distorted ($r^c_{1U}=23\%$). CDA-PARAFAC performs well ($r^c_{1CDA}=4.2\%$) but the relative error is still high for the first solution. It should be noted that ACA-PARAFAC ($r^c_{1ACA}=0.4\%$) do better than CDA-PARAFAC. This last result is surprising because it is in contradiction with the five other loadings.

Table 4
Data set 1, concentration mode results.

Fluorophore	r^c_{1R}	r^c_{1U}	r^c_{1ACA}	r^c_{1CDA}
Quinine sulphate	0.1	8.3	0.7	0.2
Fluorescein	0.08	23	0.4	4.2

Relative squared residual error in percent between the real profiles and their estimation from I_{1R} (r^c_{1R}), I_{1U} (r^c_{1U}), I_{1ACA} (r^c_{1ACA}) and I_{1CDA} (r^c_{1CDA}).

Table 5
Data set 1, excitation mode results.

Fluorophore	Criterion	Ref.	Unc.	ACA cor.	CDA cor.
Quinine sulphate	Rel. err. max. val.	0.4	24	23	0.5
	Shift	0	20	0	0
	r^{ex}	0.06	12.9	4.1	0.08
Fluorescein	Rel. err. max. val.	2.5	50.5	15	17
	Shift	0	20	5	5
	r^{ex}	0.07	95.15	9.3	3.4

Comparison with the real spectra among three criteria: relative error on the maximum value (%), shift (nm) and relative squared error (%).

Table 6
Data set 1, emission mode results.

Fluorophore	Criterion	Ref.	Unc.	ACA cor.	CDA cor.
Quinine sulphate	Rel. err. max. val.	1.4	4.1	4.1	0.7
	Shift	0	5	5	0
	r^{em}	0.06	1.8	0.17	0.1
Fluorescein	Rel. err. max. val.	3.9	4	4.7	0.6
	Shift	0	0	15	0
	r^{em}	0.4	7.6	15	0.5

Comparison with the real spectra among three criteria: relative error on the maximum value (%), shift (nm) and relative squared error (%).

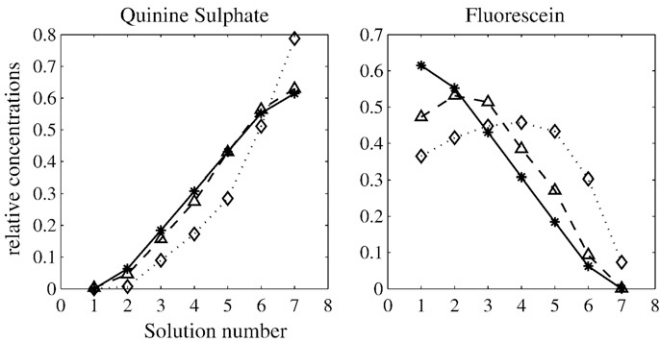

Fig. 7. Data set 1, PARAFAC loadings of the concentration mode: Real spectra (solid * line), U-PARAFAC loadings (dot ◊ line) and CDA-PARAFAC loadings (dash △ line).

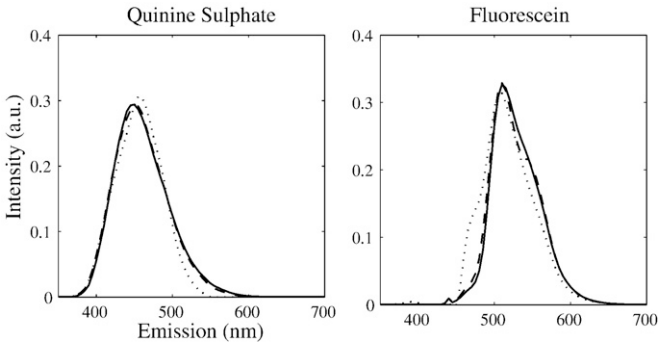

Fig. 9. Data set 1, PARAFAC loadings of the emission mode: Real spectra (solid line), U-PARAFAC loadings (dot line) and CDA-PARAFAC loadings (dash line).

Results for the excitation mode are presented in Table 5 and Fig. 8. The excitation mode is the most affected by inner filter effects, with r^{ex}_{1U} values of 12.9% and 95.15% for quinine sulphate and fluorescein respectively. Considering Fig. 8, quinine sulphate excitation spectrum is widened and flattened by inner filter effects. These distortions are completely eliminated by CDA-PARAFAC. Indeed, the CDA-PARAFAC estimated spectrum is really close to the real spectrum ($r^{ex}_{1CDA}=0.08\%$). ACA-PARAFAC ($r^{ex}_{1ACA}=4.1\%$) globally improves U-PARAFAC result ($r^{ex}_{1U}=12.9\%$). The relative error on the maximum value is negligible with CDA-PARAFAC (0.5%) while it as important with ACA-PARAFAC (23%) as without correction (24%). The 20 nm shift on the position of the maximum is perfectly corrected by both CDA-PARAFAC and ACA-PARAFAC. These observations hold true for the fluorescein spectrum but the gaps between the different estimations are wider. The spectrum estimated by U-PARAFAC is totally distorted in respect to the real spectrum, $r^{ex}_{1U}=95.15\%$. In spite of some residual distortions (flattening and widening), the spectrum shape is almost fully recovered with CDA correction ($r^{ex}_{1CDA}=3.4\%$). ACA-PARAFAC global estimation is not as good ($r^{ex}_{1ACA}=9.3\%$). In absence of correction, the relative error on the maximum value is very high (50.5%). ACA-PARAFAC and CDA-PARAFAC relative error are equivalent with 15% and 17% respectively. In the same way the maximum shift is limited by ACA-PARAFAC and CDA-PARAFAC to the fluorometer excitation step (5 nm) against 20 nm with U-PARAFAC.

Results for emission mode are presented in Table 6 and Fig. 9. The emission spectrum of quinine sulphate is well estimated by U-PARAFAC ($r^{em}_{1U}=1.8\%$). However ACA-PARAFAC and CDA-PARAFAC still improve this result in different proportions ($r^{em}_{1ACA}=0.17\%$ and $r^{em}_{1CDA}=0.1\%$). One should note that the relative error on the maximum value is the same with ACA-PARAFAC than with U-PARAFAC (4.1%). This small error is corrected by CDA-PARAFAC (0.7%). In the same way, the 5 nm shift is only corrected by CDA-PARAFAC. A closer look should be given to fluorescein spectrum. This for two reasons: Firstly, CDA-PARAFAC removes the shift of the right slope and corrects the large distortion on the left slope of the peak (Fig. 9). It also creates a weaker distortion on the right slope. This distortion is negligible but it is very similar to the spectral distortion observed on the CDA corrected FEEM of solution 1 (Fig. 6). Secondly, ACA-PARAFAC shows its real limitation on this loading as the estimated spectrum is worse than the one estimated by U-PARAFAC regarding the three criteria (Table 6). The relative squared error is twice higher (15% against 7.6%) with ACA-PARAFAC than with U-PARAFAC while it is negligible with CDA-PARAFAC (0.5%). The relative error on the maximum value is quite small with U-PARAFAC (4%) and ACA-PARAFAC (4.7%) but it is totally corrected by CDA-PARAFAC (0.7%). Eventually, ACA-PARAFAC introduces a 15 nm shift on the position of the maximum which does not exist with U-PARAFAC and CDA-PARAFAC.

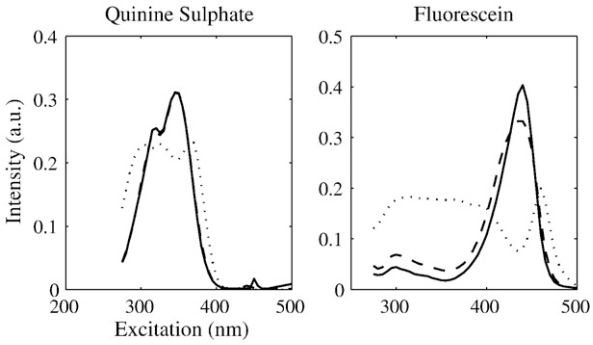

Fig. 8. Data set 1, PARAFAC loadings of the excitation mode: Real spectra (solid line), U-PARAFAC loadings (dot line) and CDA-PARAFAC loadings (dash line).

In conclusion to this test, as expected, U-PARAFAC provides the worst results. These are very bad, specially for the fluorescein excitation spectrum and quinine sulphate emission spectrum whose wavelength domains strongly overlap. ACA-PARAFAC improves these results. Regarding ACA results, loadings estimation is better than expected. However, it is outperformed by CDA-PARAFAC at the exception of the fluorescein concentration profile. CDA-PARAFAC results are indeed closer to those obtained with the reference FEEM although a larger error is observed on fluorescein excitation (Table 5) and concentration loadings (Table 6). This must be seen as the PARAFAC manifestation of the small distortion observed on the CDA correction of solution 1 (Fig. 6) and more generally this is an indication of the CDA limitations. Actually, CDA is limited to a certain domain of validation because Eq. (11) is obtained after several approximations. This holds true for any correction method relied on Eq. (11). Regarding the results of Table 3 and Fig. 7, this limitation has probably been reached with solution 1. In these cases of very high absorbance (equal or above 2), more sophisticated models should be used. Nevertheless, we have demonstrated here that the validation domain of CDA is much larger than the linear one. Then the FEEM provided by CDA are close enough to the ideal linear FEEM to allow advanced spectral data analysis such as the PARAFAC decomposition while this is not the case with uncorrected FEEM or with ACA to a lesser extent. This example also show that CDA-PARAFAC improves both kinds of PARAFAC results: On the one hand it allows to recover the overall profile of strongly distorted loadings, on the other hand it provides some very accurate estimations of less affected loadings.

4.2. Data set 2, application to field

In this section, performances of CDA and CDA-PARAFAC are shown for the correction and the decomposition of mixtures of model molecules. The first stage of the test is a comparison between the reference FEEM (I_{2R}), the uncorrected FEEM (I_{2U}) and the CDA corrected FEEM (I_{2CDA}) of data set 2. Four representative examples of these different FEEM are presented on Fig. 10. Regarding these

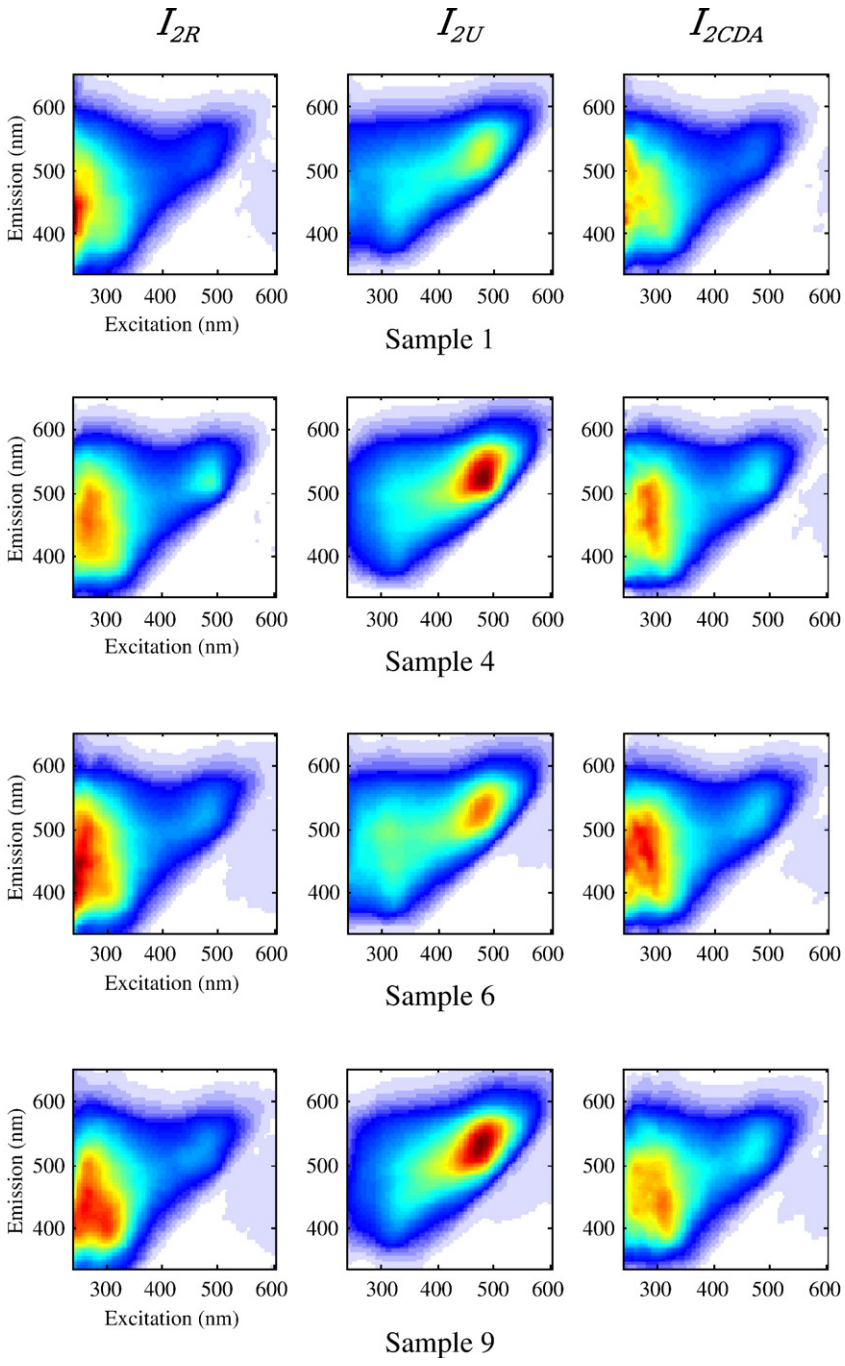

Fig. 10. Illustrations of I_{2R}, I_{2U} and I_{2CDA} for samples 1, 4, 6 and 9 of data set 2.

examples a main distortion appears on the fluorescence pattern if no correction is applied. It turns out that filter effects increase the peak around (480 nm, 520 nm) and decrease the intensity of the fluorescence signal located under 400 nm in excitation. This area is composed by several peaks which are partially recovered by CDA. The PARAFAC decompositions should show whether this finer aspect of the correction is satisfying or not. The relative squared residual error terms (r_{2U} and r_{2CDA}) of the whole data set are given in Table 7. FEEM obtained with CDA are not as closed to the reference FEEM as for data set 1. Actually, r_{2CDA} average value is about 4% while it is about 55% for r_{2U}. Hence, it proves that CDA correction is still very beneficial relatively to the uncorrected FEEM.

Table 7
Comparison of the relative squared residual error terms (in %) for the eleven solution of data set 2.

Sample	1	2	3	4	5	6	7	8	9	10	11
r_{2U}	51	66	35	59	35	44	83	76	83	10	60
r_{2CDA}	3	3	5	1.4	5	3	4	5	6	5	2

Table 8
Data set 2, concentration mode results.

Fluorophore	r^c_{2U}	r^c_{2CDA}
1	6.6	5.6
2	26	4
3	7.3	8.2

Relative squared residual error in percent between the reference loadings and U-PARAFAC loadings (r^c_{2U}) or CDA-PARAFAC loadings (r^c_{2CDA}).

Table 9
Data set 2, excitation mode results.

Fluorophore	Test	Unc.	CDA cor.
1	Rel. err. max. val.	18	11
	Shift	185	15
	r^{ex}	110	1.5
2	Rel. err. max. val.	30	20
	Shift	20	0
	r^{ex}	9.6	2.1
3	Rel. err. max. val.	27.5	0.2
	Shift	10	5
	r^{ex}	35	0.6

Comparison with the reference loadings among three criteria: relative error on the maximum value (%), shift (nm) and relative squared error (%).

Table 10
Data set 2, emission mode results.

Fluorophore	Test	Unc.	CDA cor.
1	Rel. err. max. val.	13	12
	Shift	40	25
	r^{em}	21	4
2	Rel. err. max. val.	21	1.8
	Shift	60	10
	r^{em}	63	6
3	Rel. err. max. val.	5.2	1.4
	Shift	20	10
	r^{em}	8.8	0.9

Comparison with the reference loadings among three criteria: relative error on the maximum value (%), shift (nm) and relative squared error (%).

The PARAFAC-ALS algorithm was applied to I_{2R}, I_{2U} and I_{2CDA}. In opposition to set 1, the real number of fluorophore is unknown. This is actually the main problem with PARAFAC analysis of unknown FEEM. We compared the results provided by three classical tests: residual variance analysis, split half analysis and CORCONDIA. Finally, three components were used for the decompositions. These will be labelled fluorophore 1, 2 and 3 in the following. The real fluorophores are also unknown, consequently, R-PARAFAC loadings are taken as references for the evaluation of U-PARAFAC and CDA-PARAFAC results. This comparison is made on Tables 8–10 and Figs. 11–13.

Results for the concentration mode are presented in Table 8 and Fig. 11. Inner filters and CDA correction have little effects on the profile of fluorophore 1 ($r^c_{2U}=6.6\%$ and $r^c_{2CDA}=5.6\%$) and 3 ($r^c_{2U}=7.3\%$ and $r^c_{2CDA}=8.2\%$). On the opposite, fluorophore 2 is far more affected. The concentration profile estimated by U-PARAFAC is clearly unsatisfying ($r^c_{2U}=26\%$). CDA-PARAFAC provides an acceptable estimation as the error term decreases to 4%. Finally the three estimated profiles by CDA-PARAFAC are satisfying at the exception of samples 8 and 9. At the opposite of r^c_{2U}, r^c_{2CDA} is greater for fluorophores 1 and 3. This is mainly due to the larger estimation errors on samples 8 and 9.

Results for excitation mode are presented in Table 9 and Fig. 12. Excitation mode is the most affected mode of the decomposition as for data set 1. Estimation of fluorophore 1 excitation spectrum takes a clear advantage of CDA-PARAFAC. Regarding shape and position, the spectrum estimated by U-PARAFAC is a far cry from the reference spectrum ($r^{ex}_{2U}=110\%$). On the opposite, CDA-PARAFAC provides a very good estimation ($r^{ex}_{2CDA}=1.5\%$). The relative error on the maximum value is smaller (11% against 18%) but above all, the large shift (185 nm) is brought back to 15 nm. Despite U-PARAFAC estimation of fluorophore 2 spectrum is acceptable ($r^{ex}_{2U}=9.6\%$), CDA-PARAFAC improves this result ($r^{ex}_{2CDA}=2.1\%$). In the absence of correction, the double peak disappears. CDA-PARAFAC correctly restores this feature but the relative error on the maximum value remains high (20%). On the other hand, the 20 nm shift is completely corrected. U-PARAFAC estimation of fluorophore 3 spectrum is not satisfying ($r^{ex}_{2U}=35\%$). One of the two peaks almost disappears while the second one is overestimated. Nevertheless, its estimation by CDA-PARAFAC is almost identical to the reference spectrum ($r^{ex}_{2CDA}=0.6\%$). The relative error on the maximum value is significant with U-PARAFAC (27.5%) but it becomes negligible with CDA-PARAFAC (0.2%). The shift is also reduced from 10 nm to 5 nm.

Results for emission mode are presented in Table 10 and Fig. 13. Estimation of fluorophore 1 emission spectrum by U-PARAFAC is mitigated ($r^{em}_{2U}=21\%$). CDA-PARAFAC overall result is very acceptable ($r^{em}_{2CDA}=4\%$). The spectrum is overestimated by both U-PARAFAC (relative error to the maximum value of 13%) and CDA-PARAFAC (12%). On the opposite, CDA-PARAFAC limits to 25 nm the large shift (40 nm) observed when no correction is applied. Fluorophore 2 spectrum is more severely affected by inner filter effects. CDA-PARAFAC provides a very satisfying estimation of this spectrum ($r^{em}_{2CDA}=6\%$) in respect to U-PARAFAC result ($r^{em}_{2U}=63\%$). The relative error to the maximum value observed with U-PARAFAC is important (21%) but it is well corrected by CDA-PARAFAC (1.8%). In the same way, the 60 nm shift is limited to 10 nm. Fluorophore 3 spectrum is correctly estimated by U-PARAFAC ($r^{em}_{2U}=8.8\%$). CDA-PARAFAC still improves the estimation ($r^{em}_{2CDA}=0.9\%$). The relative error to the maximum value is lower (1.4% against 5.2%) and the shift is reduced from 20 nm to 10 nm.

CDA-PARAFAC results on data set 2 are also conclusive. All the loadings are indeed correctly estimated. Relative concentrations of only one fluorophore in only two samples out of eleven are poorly

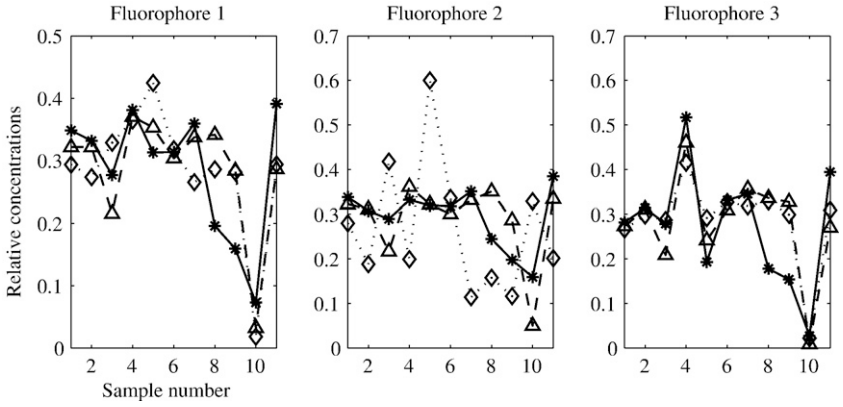

Fig. 11. Data set 2, PARAFAC loadings of the concentration mode: R-PARAFAC loadings (solid * line), U-PARAFAC loadings (dot ◊ line) and CDA-PARAFAC loadings (dash △ line).

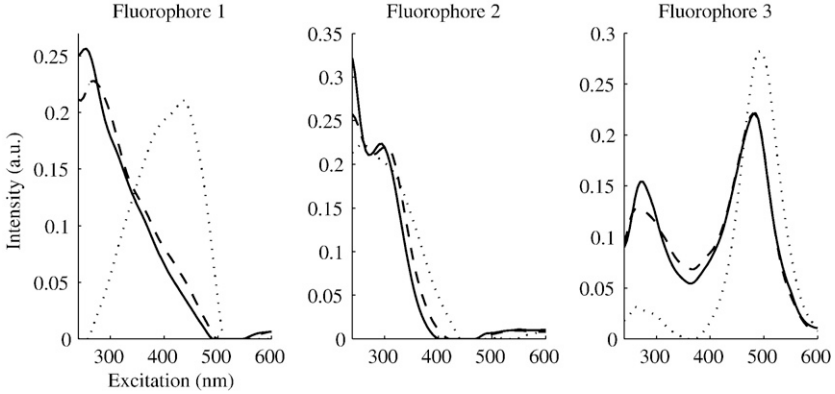

Fig. 12. Data set 2, PARAFAC loadings of the excitation mode: R-PARAFAC loadings (solid line), U-PARAFAC loadings (dot line) and CDA-PARAFAC loadings (dash line).

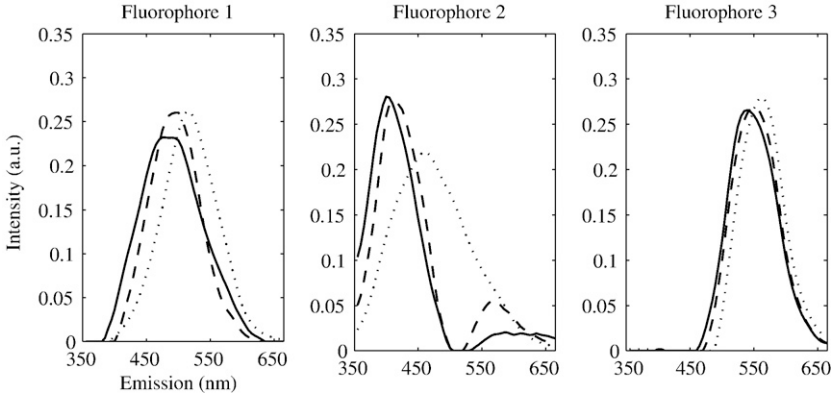

Fig. 13. Data set 2, PARAFAC loadings of the emission mode: R-PARAFAC loadings (solid line), U-PARAFAC loadings (dot line) and CDA-PARAFAC loadings (dash line).

estimated and all the estimated spectra are close enough to the corresponding reference spectra. The crucial point on this second example is that in a real case situation of DOM tracing, CDA-PARAFAC would probably give interpretative results while the uncorrected FEEM would provide misleading estimations. Moreover, excitation spectra of fluorophores 1 and 3 illustrate the two main kinds of spectral deviations due to inner filters. Fluorophore 1 shape is distorted and its position is shifted from 275 nm to 480 nm. On the opposite, the position of fluorophore 3 is unchanged, its global shape is almost correct but the respective magnitude of its two peaks is largely modified. CDA-PARAFAC provides an impressive correction of both deviations.

Actually, CDA-PARAFAC appears to be a critical improvement of U-PARAFAC or even ACA-PARAFAC in the case of strong inner filter effects.

5. Conclusion

It is possible to correct inner filter effects by using simply a Controlled Dilution Approach (CDA). This analytical solution is better than usual absorbance correction and quicker and safer than strong dilution, under absorbance of 0.1. It has been demonstrated in this work the good ability of CDA and CDA-PARAFAC in the case of standard mixtures of two fluorophores and in the case of real DOM samples. In this study, CDA performed very well for solution absorbances up to 1.83. Further investigation should be made outside this range. We conjecture that another theoretical model of fluorescence measurement should be used for absorbance higher than 2.

In respect to the PARAFAC decomposition, better results were obtained on the spectral loadings. We have also highlighted the limit of ACA for the correction of strong filter effects. Consequently, we recommend the use of CDA for FEEM experiment and PARAFAC pretreatment to avoid error and misinterpretation.

References

[1] B. Valeur, Molecular Fluorescence. Principles and Applications, Wiley-VCH, Weinheim, 2002.
[2] A. Hansch, D. Sauner, I. Hilger, J. Böttcher, A. Malich, O. Frey, R. Bräuer, W.A. Kaiser, Academic Radiology 11 (11) (2004) 1229–1236.
[3] E. Sikorska, T. Gorecki, I.V. Khmelinskii, Sikorski, D. de Keukeleire, Food Chemistry 96 (4) (2006) 632–639.
[4] G.P. Coble, Marine Chemistry 51 (1996) 325–346.
[5] C.A. Stedmon, S. Markager, Limnology and Oceanography 50 (2) (2005).
[6] J.R. Lakowicz, Principles of Fluorescence Spectroscopy, Plenum Press, NY, 1983.
[7] C.A. Parker, W.J. Barnes, The Analyst 82 (1957) 606–618.
[8] J.J. Mobed, S.L. Hemmingsen, J.L. Autry, L.B. McGown, Environmental Science and Technology 30 (10) (1996) 3061–3065.
[9] J.F. Holland, R.E. Teets, P.M. Kelly, A. Timnick, Analytical Chemistry 49 (6) (1977) 706–710.
[10] C.M. Yappert, J.D. Ingle, Applied Spectroscopy 43 (5) (1989) 759–767.
[11] S.A. Tucker, V.L. Amszi, W.E. Acree, Journal of Chemical Education 69 (1992).
[12] B.C. MacDonald, S.J. Lvin, H. Patterson, Analytica Chimica Acta 338 (1997) 155–162.
[13] A. Credi, L. Prodi, Spectrochimica Acta Part A 54 (1998) 159–170.
[14] J. Riesz, J. Gilmore, P. Meredith, Spectrochimica Acta Part A (2004).
[15] T. Ohno, Environmental Science and Technology 36 (4) (2002) 742–746.
[16] D.M. MacKnight, E.W. Boyer, P.K. Westerhoff, P.T. Doran, T. Kulbe, D.T. Andersen, Limnology and Oceanography 46 (2001) 38–48.
[17] F. Cuesta Sanchez, S. Rutan, M. Gil Garcia, D. Massart, Chemometrices and Intelligent Laboratory Systems 36 (1997) 153–164.
[18] A. Garrido Frenich, D. Picon Zamora, J. Martinez Vidal, M. Martinez Galera, Analytica Chimica Acta 449 (2001) 143–155.
[19] J. Boehme, P. Coble, R. Conmy, A. Stovall-Leonard, Marine Chemistry 89 (2004) 3–14.
[20] J.M. Andrade, M.P. Gomez-Carracedo, W. Krzanowsky, M. Kubista, Chemometrices and Intelligent Laboratory Systems 72 (2004) 123–132.
[21] R.A. Harshman, UCLA Working Papers in Phonetics 16 (1970) 1–84 (UMI Serials in Microform, No. 10,085).
[22] R. Bro, Chemometrics and Intelligent Laboratory Systems 38 (1997) 149–171.
[23] C.A. Stedmon, S. Markager, R. Bro, Marine Chemistry 82 (3–4) (2003) 239–254.

[24] R.D. Holbrook, J.H. Yen, T.J. Grizzard, Science of the Total Environment 361 (1–3) (2006) 249–266.
[25] X. Luciani, S. Mounier, H.H.M. Paraquetti, R. Redon, Y. Lucas, A. Bois, L.D. Lacerda, M. Raynaud, M. Ripert, Marine Environmental Research 65 (2) (2008) 148–157.
[26] D. Baunsgaard, Department of Dairy and Food Science, The Royal Veterinary and Agricultural University, (1999).
[27] G.G. Anderson, K.D. Brian, K.S. Booksh, Chemometrics and Intelligent Laboratory Systems 49 (1999) 195–213.
[28] O. Divya, A.K. Mishra, Analytica Chimica Acta 630 (2008) 47–56.
[29] P. John, I. Soutar, Analytical Chemistry 48 (1976) 520–524.
[30] D. Patra, A.K. Mishra, Analyst 125 (2000) 1383–1386.
[31] R.A. Harshman, UCLA Working Papers in Phonetics 22 (1972) 111–117 (UMI Serials in Microform, No. 10,085).
[32] N.D. Sidiropoulos, R. Bro, Journal of Chemometrics 14 (3) (2000) 229–239.
[33] N.M. Faber, R. Bro, P.K. Hopke, Chemometrics and Intelligent Laboratory Systems 65 (2003) 119–137.
[34] G. Tomasi, R. Bro, Computational Statistics & Data Analysis 50 (7) (2006) 1700–1734.
[35] P. Paatero, Chemometrices and Intelligent Laboratory Systems 38 (2) (1997) 223–242.
[36] R.A. Harshman, M.E. Lundy, Computational Statistics & Data Analysis 18 (1994) 39–72.
[37] C. Andersen, R. Bro, Journal of Chemometrics 17 (2003) 200–215.
[38] R.G. Zepp, W.M. Sheldon, M.A. Moran, Marine Chemistry 89 (2004) 15–36.
[39] C.A. Andersson, R. Bro, Chemometrics and Intelligent Laboratory Systems 52 (2002) 1–4.
[40] R. Bro, H.A.L. Kiers, Journal of Chemometrics 17 (2003) 274–286.